JOURNAL OF MATERIALS SCIENCE 33 (1998) 3655–3659

Photoelectrochemical properties of sol–gel-derived anatase and rutile TiO_2 films

GAOLING ZHAO
Department of Material Science and Engineering, Zhejiang University, Hangzhou, 310027, People's Republic of China

S. UTSUMI, H. KOZUKA, T. YOKO
Institute for Chemical Research, Kyoto University, Gokasho, Uji-shi, Kyoto-fu, 611-0011, Japan
E-mail: yokot@vidrio.kuicr.kyoto-u.ac.jp

Anatase and rutile film electrodes with comparable porosities were prepared by the sol–gel dip-coating method, and the photoelectrochemical properties were studied based on photocurrent measurement and impedance analysis in a three-electrode wet cell. The photocurrent was found to increase with the donor density, both in anatase and rutile electrodes. For the same donor density, however, rutile electrodes exhibited higher photocurrents than anatase electrodes, which was ascribed to the more beneficial bandgap structure of the former. © *1998 Kluwer Academic Publishers*

1. Introduction

TiO_2 has enjoyed tremendous popularity as a semiconductor photoelectrode because of its prominent chemical and electrochemical stability. Various methods have been employed to prepare TiO_2 film electrodes, for example, chemical vapour deposition [1], anodization of titanium metal [2], thermal oxidation of titanium metal [3], r.f. sputtering [4], and arc-plasma spraying [5].

Very recently, the sol–gel process has attracted much attention as a film formation process because it offers a number of advantages, such as low-temperature processing, easy material definition at the molecular level, easy production of large size film with a controlled specific surface area and the formation of metastable crystalline or amorphous phase. The sol–gel-derived TiO_2 films with high specific surface area exhibit large photocurrents [6–9] and dye-sensitized photocurrents [10, 11] because of the possible adsorption of large amounts of oxygen and water molecules and dye molecules. Furthermore, because a homogeneous solution is employed in the sol–gel process as the starting material, and a porous gel with a controlled pore size is the intermediate, homogeneous distribution of metal cations and dispersion of size-controlled semiconductor or metal particles can be achieved in sol–gel-derived oxide electrodes, realizing visible light sensitization [12, 13].

As far as the crystalline phase is concerned, anatase has the advantage for the photoelectrochemical energy conversion, because it has a higher adsorptive activity for oxygen and water than rutile [14, 15]. From this viewpoint, the sol–gel process can be said to have a notable advantage, because it provides a route to high surface area anatase TiO_2 film, being a low-temperature process. From the standpoint of the optical bandgap, however, the anatase has a disadvantage, because it shows an indirect interband transition and has a larger optical bandgap ($E_g = 3.2\,eV$) [16] than rutile ($E_g = 3.0\,eV$) [17].

At the moment it is not known exactly how the crystalline phase, rutile or anatase, affects the photoelectrochemical energy conversion efficiency of the TiO_2 electrodes as mentioned above. Although comparison between rutile and anatase electrodes seems interesting, it should be remembered that other parameters affect the energy conversion process, such as donor density and porosity. In other words, electrode samples with comparable porosities and donor densities should be prepared in order to clarify the effect of the crystalline phase. In the present study, rutile and anatase film electrodes were prepared by the sol–gel method, where the donor density and porosity were varied by varying the heat-treatment conditions. In order to study the effect of the crystalline phase, the photoelectrochemical properties were compared between samples with comparable porosities and donor densities.

2. Experimental procedure

2.1. Sample preparation

The TiO_2 film electrodes were prepared by the sol–gel dip-coating method. A starting solution of a molar composition, $Ti(OC_3H_7^i)_4 : H_2O : C_2H_5OH : HNO_3 = 1 : 1 : 10 : 0.2$, was prepared. In order to achieve homogeneous hydrolysis and to avoid precipitation, a solution of water and nitric acid diluted with half of the prescribed amount of ethanol, was added dropwise to titanium isopropoxide diluted with the remaining

ethanol under vigorous stirring at 0 °C. The solution was stirred at 25 °C for 2 h. A cleaned Nesa silica glass substrate was dipped into the solution and withdrawn at a constant rate of 1 mm s^{-1} and then annealed at a temperature ranging between 400 and 600 °C for 10 min. The dip-coating and the annealing were repeated ten times in order to obtain thicker film electrodes. Finally, a post-annealing was carried out in the temperature range between 600 and 900 °C for different times to control the porosity of the film electrodes.

2.2. Characterization

The crystalline phase of the samples was identified by X-ray diffraction (XRD) by means of a Rigaku RAD II X-ray diffractometer by using the Cu K_α line. The refractive indices of the samples were determined by means of a Mizojiri Optical Works Model DVA-36VW ellipsometer at a wavelength of 633 nm.

2.3. Photoelectrochemical measurements

The current–potential curves of the TiO_2 film electrodes in contact with a buffer solution of pH 7 containing 0.2 M $Na_2B_4O_7$, 0.14 M H_2SO_4, and 0.3 M Na_2SO_4 were obtained by means of a Hokuto Denko HA-501 M potentiostat. An Ushio Denki 500 W xenon lamp was used for irradiating the electrode samples.

In order to determine the donor density and the film resistance, impedance analysis was carried out in the dark in the same buffer solution at 1kHz by an HZ-1A electrochemical impedance measurement system composed of an HA-501 M potentiostat and an NF Circuit Block FRA-5090 frequency reponse analyser.

3. Results and discussion

3.1. Crystallization and porosity of the film electrodes

XRD results showed that the electrode samples were single-phase anatase and rutile when the post-annealing temperature $T_{pa} \leqslant 700$ °C and $T_{pa} \geqslant 800$ °C, respectively, as summarized in Table I.

In order to determine the relationship between the electrode sample porosity and the annealing parameters, the porosity was measured for the electrode samples prepared under various annealing conditions. The porosity of the samples was calculated from the refractive indices by the following expression [18]

$$p = 1 - \frac{1 - n^2}{1 - n_d^2} \quad (1)$$

where p is the porosity, and n and n_d are the refractive indices of the film and the corresponding crystalline form, respectively. The refractive indices of anatase and rutile crystals employed in the calculation were 2.513 and 2.676, respectively [19].

The porosities are shown in Fig. 1 as a function of the post-annealing time for the electrode samples prepared under various annealing conditions. The porosity of the anatase samples remained unchanged with the post-annealing time when T_{pa} was 600 °C, and decreased at $T_{pa} = 700$ °C. The porosity decreased drastically at $T_{pa} \geqslant 800$ °C in the initial post-annealing stage, accompanied by anatase–rutile transformation. The porosity of the rutile samples also decreased with the post-annealing time.

3.2. Electrical and photoelectrochemical properties of the film electrodes

In order to clarify the effect of the crystalline phase on the photoelectrochemical properties in later sections, the electrode samples with comparable porosities,

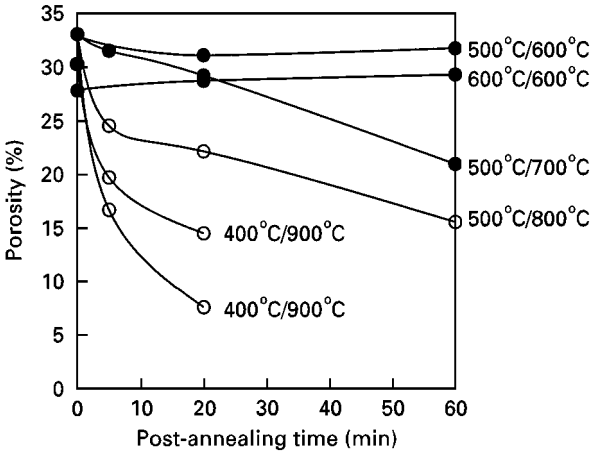

Figure 1 Porosity as a function of the post-annealing time for the TiO_2 film samples prepared at various temperatures of the repeated annealing and the post-annealing. The temperatures denoted in the figure are those employed in the repeated annealing and the post-annealing. (●) Anatase, (○) rutile phases.

TABLE I Repeated annealing and post-annealing conditions, crystalline phase, porosity, donor density, and photocurrent of the samples

Sample name	Repeated annealing temp. (°C)	Repeated annealing time (min)	Post-annealing temp. (°C)	Post-annealing time (min)	Crystalline phase	Porosity (%)	Donor density (10^{25} m^{-3})	Photocurrent at 1 V versus SCE (Am^{-2})	Film resistance (Ω)
A-27-1	600	10	600	22	Anatase	27	1.59	71	246
A-27-2	500	10	700	22	Anatase	27	1.97	90	240
A-22	500	10	700	54	Anatase	22	0.09	55	466
R-22	500	10	800	20	Rutile	22	0.64	85	238
R-20-1	500	10	800	36	Rutile	20	0.17	60	340
R-20-2	400	10	900	5	Rutile	20	0.92	86	218

as listed in Table I, were selected for the photoelectrochemical measurements.

3.2.1. Resistance and donor density of the film electrodes

Film resistance and space charge layer capacitance were measured by an impedance analysis.

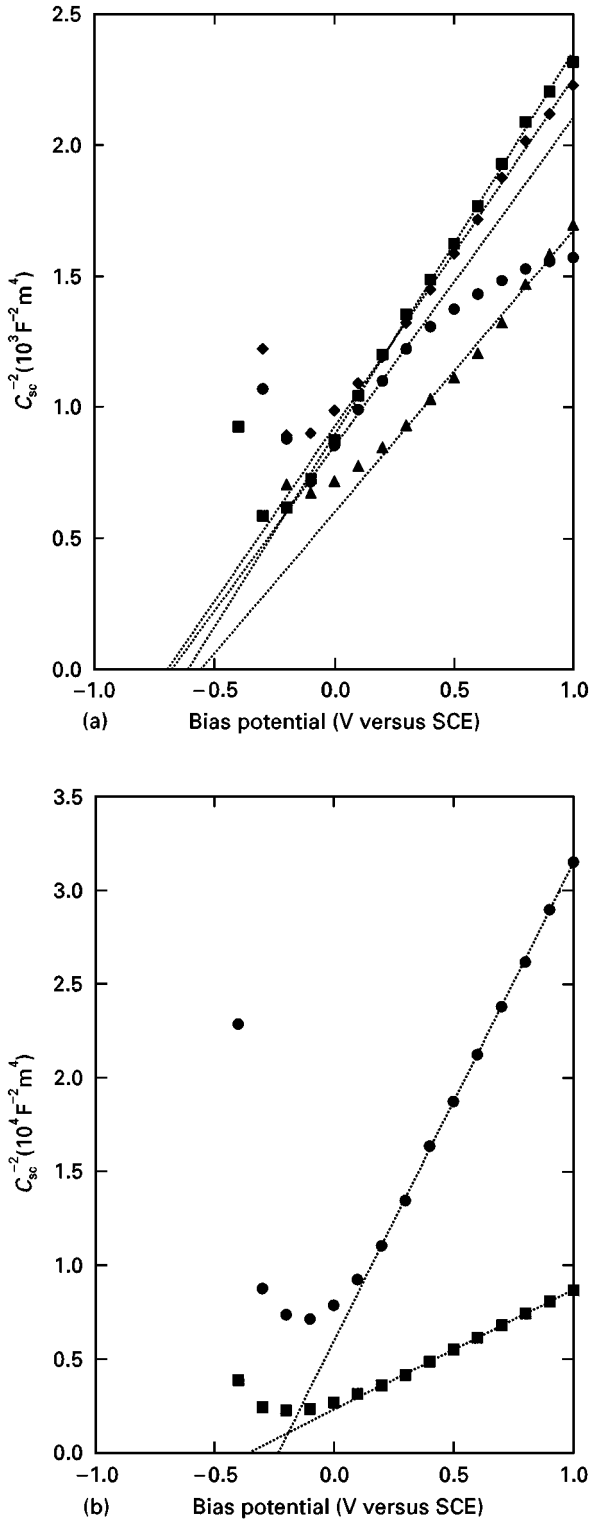

Figure 2 Mott–Schottky plot for the electrode samples. The plot is separated into two figures because of the large difference in magnitude of the data. (a) (●) R-20-2, (■) R-22, (◆) A-27-1, (▲) A-27-2; (b) (■) R-20-1, (●) A-22.

Donor density of the electrode samples was determined by the Mott–Schottky equation [20]

$$C_{sc}^{-2} = \frac{2}{e\varepsilon\varepsilon_0 N_D}\left[(V - V_{fb}) - \frac{kT}{e}\right] \quad (2)$$

where C_{sc} is the space charge layer capacitance, N_D the donor density, V_{fb} the flatband potential versus a Standard Calorial Electrode (SCE), and V the bias potential versus SCE, all of which are of the working electrode, i.e. of the electrode sample. e is the electronic charge, ε the TiO_2 permittivity (55 for anatase [21] and 100 for rutile [22], ε_0 the permittivity of vacuum, and k the Boltzmann constant. Linear relationships were obtained between C_{cs}^{-2} and V in the region from -0.2 to 1.0 V versus SCE as shown in Fig. 2, and the donor density was obtained from the slope of the linear part of the plot.

The resistance and the donor density thus obtained for the samples with comparable porosity are listed in Table I. Fig. 3 shows the relation between the donor density and resistance. It is seen that the resistance decreases with increasing donor density for both anatase and rutile electrodes.

As seen in Table I, the donor density was varied with the post-annealing parameters. It is well accepted that Ti^{3+} ions act as the donors in sol–gel-derived TiO_2 electrodes, which are formed by reduction of Ti^{4+} ions via thermal decomposition and oxidation of the organic residues [23]. Generally, moderately high temperatures are required for decomposing organics, which allows Ti^{3+} formation, but reoxidation of Ti^{3+} into Ti^{4+} occurs at higher temperatures or on longer annealing [23]. For the present anatase samples, higher donor densities were achieved when the post-annealing was performed at a higher T_{pa} of 700 °C

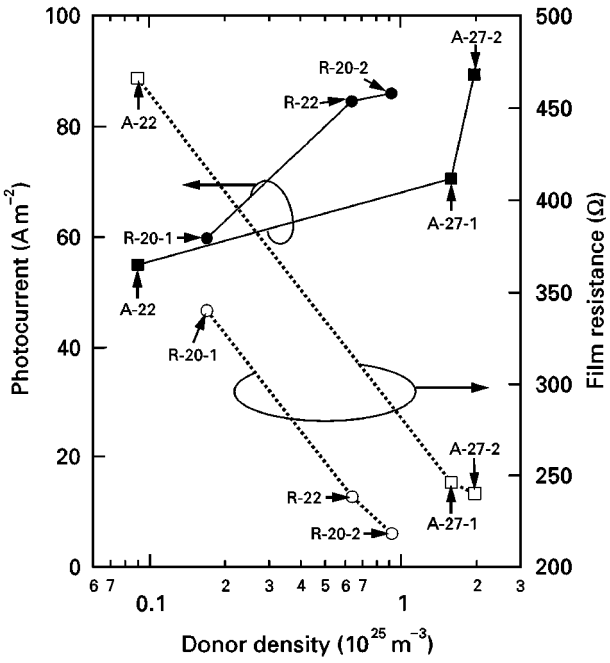

Figure 3 Photocurrent and resistance as a function of the donor density for the film electrode samples listed in Table I.

(compare A-27-1 and A-27-2 in Table I). Longer post-annealing at this temperature, however, decreased the donor density and increased the resistance (compare A-27-2 and A-22 in Table I). Because the rutile phase formation was achieved at higher T_{pa} than the anatase, the donor densities, i.e. Ti^{3+} concentrations, were lower in the rutile samples.

3.2.2. Effect of the donor density on the photoelectrochemical properties

I–V curves are shown in Figs. 4 and 5 for the rutile and anatase electrodes with comparable porosity, respectively, and the photocurrents at 1 V versus SCE are summarized in Table I. It is seen that the photocurrent values changed by the annealing parameters. The photocurrent at 1 V versus SCE is plotted against the donor density in Fig. 3. It is seen that the photocurrent increases with donor density, i.e. Ti^{3+} ion concentrations, in rutile and anatase electrodes. First, higher donor densities can lower the bulk resistance, enhancing the photocurrent. Second, because Ti^{3+}–H_2O and Ti^{3+}–OH^- at the TiO_2 surface can act as the photoredox reactions as discussed previously [8], Ti^{3+} species at the electrode surface can also contribute to the photocurrent enhancement.

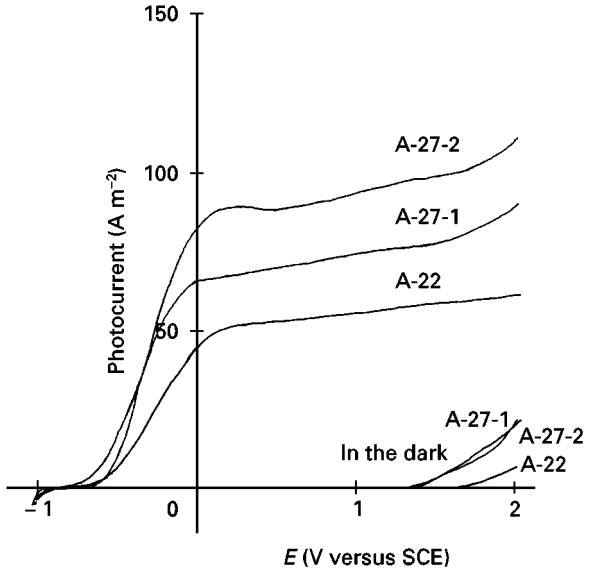

Figure 4 Photocurrent–potential curves of the anatase electrode samples.

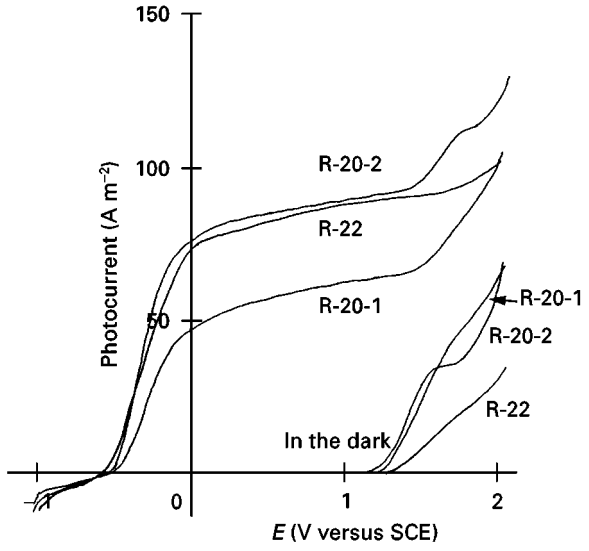

Figure 5 Photocurrent–potential curves of the rutile electrode samples.

3.2.3. Effect of the crystalline phase on the photoelectrochemical properties

Comparing Figs. 4 and 5, it is clear that, for the rutile electrodes, the cathodic current begins to flow at the onset potential of the photoanodic currents, whereas for the anatase electrodes there exists a potential range where neither cathodic nor anodic current flows, indicating that the cathodic performance of the rutile films is better than that of the anatase ones.

Fig. 6 compares the *I–V* curves for the rutile and the anatase film electrodes having the same porosity, clearly showing that the rutile electrode exhibits a higher photocurrent than the anatase electrode. As mentioned in Section 3.2.2, the photocurrent increased with the donor density for both rutile and anatase film electrodes. As seen in Table I, however, the rutile electrode, even with lower donor density, exhibits higher photocurrent than the anatase electrode with higher donor density (compare A-27-1, R-22 and R-20-2 in Table I). This may indicate that rutile electrodes show better photoelectrochemical performance over the anatase electrodes when the donor density and porosity are the same. The structure of the optical bandgap can explain this result. Comparing with anatase ($E_g = 3.2$ eV), rutile has a narrower bandgap ($E_g = 3.0$ eV), absorbing light over a wider range of wavelength. In addition, it was previously reported [23] that sol–gel-derived rutile samples have a direct bandgap as well as an indirect bandgap, while anatase samples have an indirect bandgap. The optical

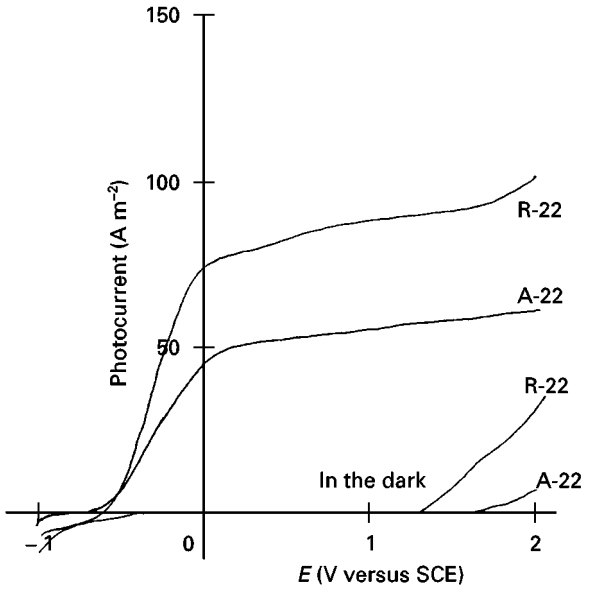

Figure 6 Photocurrent plotted against donor density for the anatase and the rutile electrode samples with the same porosity.

absorption coefficient rises more steeply with increasing photon energy for a direct band transition than an indirect one ([20] p. 7) indicating that direct bandgap semiconductors are more efficient in absorbing xenon lamp white light near the electrode/electrolyte interface. This also offers the rutile electrodes an advantage for the photoelectrochemical energy conversion.

If we can prepare rutile electrodes at T_{pa} as low as 700 °C, higher donor densities and higher porosities are expected. Such a rutile electrode with high donor density and higher porosity would exhibit higher photocurrents. In order to realize the rutile formation at lower T_{pa} however, the starting solution chemistry such as the selection of the solvent [24] should be changed and controlled.

4. Conclusions

Anatase and rutile film electrodes with comparable porosities were prepared by the sol–gel method, and the I–V curve measurement and impedance analysis was conducted in a three-electrode wet cell.

1. The photocurrent increased with donor density in the anatase and the rutile electrodes.

2. For the same porosity and donor density, the rutile electrodes exhibited higher photocurrents than the anatase electrodes. This was ascribed to the more beneficial bandgap structure of rutile.

References

1. YA. L. KOGAN and A. M. VAKULENKO, *Solar Energy Mater.* **3** (1980) 357.
2. P. CLECHET, C. MARTELET, R. OLIER, J. P. THOMAS and M. FALLAVIER, *J. Electrochem. Soc.* **130** (1983) 1795.
3. A. MONNIER and J. AUGUSTYNSKI, *ibid.* **127** (1980) 1576.
4. K. KOBAYASHI, Y. AIKAWA and SUKIGARA, *J. Appl. Phys.* **54** (1983) 2526.
5. A. A. SOLIMAN and J. J. SEGUIN, *Can. J. Phys.* **59** (1981) 1674.
6. T. YOKO, K. KAMIYA and S. SAKKA, *J. Elecroanal. Chem.* **209** (1986) 399.
7. *Idem*, *Denki Kagaku* (*J. Electrochem. Soc. Jpn*) **54** (1986) 284.
8. *Idem*, in "Ceramics Today – Tomorrow's Ceramics", edited by P. Vincenzini (Elsevier, Amsterdam, 1991) p. 2581.
9. *Idem*, *Yogyo-Kyokai-Shi* (*J. Ceram. Soc. Jpn*) **95** (1987) 150.
10. B. O'REGAN and M. GRATZEL, *Nature* **353** (1991) 737.
11. M. K. NAZERUDDIN, A. KAY, I. RODICIO, R. HUMPHRY-BAKER, E. MULLER, P. LISKA, N. VLACHOPOULOS and M. GRATZEL *J. Am. Chem. Soc.* **115** (1993) 6382.
12. G. ZHAO, H. KOZUKA and T. YOKO, *Thin Solid Films* **277** (1996) 147.
13. S. DOEUFF and C. SANCHEZ, *C. R. Acad. Sci. II, Mec. Phys. Chim. Sci. Terre.* **309** (1989) 1137.
14. A. H. BOOSTRA and C. A. H. A. MUTSAERS, *J. Phys. Chem.* **79** (1975) 1940.
15. C. D. JAEGER and A. J. BARD, *ibid.* **84** (1979) 3146.
16. H. TANG, H. BERGER, P. E. SCHMID, F. LEVY and G. BURRI, *Solid State Commun.* **87** (1993) 847.
17. J. PASCUAL, J. CAMASSEL and H. MATHIEU, *Phys. Rev.* **B 18** (1978) 5606.
18. B. E. YOLDAS and P. W. PARTLOW, *Thin Solid Films* **129** (1985) 1.
19. T. HASHIMOTO, T. YOKO and S. SAKKA, *Bull. Chem. Soc. Jpn* **67** (1994) 653.
20. H. O. FINKLEA, in "Semiconductor Electrodes", ed. by H. O. Finklea, (Elsevier, Amsterdam, 1988) p. 27.
21. R. VAN DE KROL, A. GOOSSENS, and J. SCHOONMAN, *J. Electrochem. Soc.* **144** (1997) 1723.
22. I. BURN, in "Engineered Materials Handbook", Vol. 4, edited by S. J. Schneider Jr (ASM International, USA, 1991) p. 1112.
23. T. YOKO, A. YUASA, K. KAMIYA and S. SAKKA, *J. Electrochem. Soc.* **138** (1991) 2308.
24. L. HU, T. YOKO, H. KOZUKA and S. SAKKA, *Thin solid Films* **219** (1992) 18.

Received 9 April 1997
and accepted 22 April 1998